

Tooth surface Hobbing analysis for unconventional gears with ultrasonic-assisted motion

Chunjiang He¹, Chao Lin²

¹School of Mechanical and Power Engineering, Chongqing University of Science and Technology, Chongqing, 401331, China

²College of Mechanical and Vehicle Engineering, Chongqing University, Chongqing, 400044, China

¹Corresponding author

E-mail: ¹1125135719@qq.com, ²20112407@cqu.edu.cn

Received 23 November 2021; received in revised form 14 June 2022; accepted 18 August 2022

DOI <https://doi.org/10.21595/jve.2022.22313>



Copyright © 2022 Chunjiang He, et al. This is an open access article distributed under the Creative Commons Attribution License, which permits unrestricted use, distribution, and reproduction in any medium, provided the original work is properly cited.

Abstract. As an atypical conventional gear pair, non-circular gear has a variable transmission ratio, which can be used to improve the structure and transmission characteristics in some applications, such as variable speed grinding mechanism, wool blending machine guide mechanism, continuously variable transmission structure and so on. According to the friction theory of conjugate surfaces, the transmission characteristics will be affected by the micro topography of tooth surface, but the shaped tooth surface of non-circular gear with normal hobbing method is not uniform, because of its variable radius and flank orientations of tooth surface. The research on the relationship between micro topography and parameters of non-circular gear is necessary, thus an improved manufacturing method with ultrasonic-assisted motion was presented in this paper, the mathematical equations for the theoretical tooth surface of non-circular gear with and without ultrasonic-assisted motion have been derived in this paper, also the equations for cutting parameters (step displacement, step rotating angle) have been proposed, shown that all the parameters (initial parameters of gear and gear hob, cutting parameters in manufacturing process) will affect the formed micro surfaces. In detail, the height H_m and width S_m of micro undulating tooth surface periodically increase and decrease, getting the maximum value at $\theta_n = \pi$, where is the maximum radius. The height H_m and width S_m of micro tooth surface will increase with any control parameter increase, the height H_m of most micro peaks is near 6.5um in normal hobbing process. While, the tooth surface with ultrasonic-assisted motion is more regular and clearer with the maximum height H_m decrease from 6.5 um to 2.7 um, getting more compact cutting tracks and lower surface roughness. The experimental results shows that ultrasonic-assisted hobbing has obviously positive influence for micro tooth surface, provides the theoretical support for a further analysis and better application of unconventional gear pair.

Keywords: ultrasonic-assisted motion, gear hobbing, micro tooth surface, non-circular gear, material removal.

Nomenclature

θ_p	The angle of tooth profile at point P of gear hob
θ_2	The angle between movable coordinate $O_2'-X_2'Y_2'Z_2'$ and fixed $O_2-X_2Y_2Z_2$
θ_n	Rotating angle of equivalent external gear hob at cutting point h
$ r_{bp} $	The modulus of vector r_{bp}
Δd	The step distance of adjacent cut position on gear hob
θ_{op}	The starting angle of tooth profile of gear hob
$\Delta\theta_1$	Difference of rotating angle θ_1 between two adjacent cutting steps
θ_h	Rotating angle of equivalent external gear hob at cutting point h
E	Vector of translation distance between coordinate $O_3-X_3Y_3Z_3$ and fixed $O_2-X_2Y_2Z_2$
β_3	The rotating angle of movable coordinate $O_3'-X_3'Y_3'Z_3'$
$r_p^{(3')}$	Radius of gear hob at point P in coordinate $O_3-X_3Y_3Z_3$
θ_1	The angle between movable coordinate $O_1'-X_1'Y_1'Z_1'$ and fixed $O_1-X_1Y_1Z_1$
a	Scale factor for the radius of non-circular gear
e	Eccentricity for the radius of non-circular gear

n	Orders for the radius of non-circular gear
D_X	The translation distance of coordinate $O'_2-X'_2Y'_2Z'_2$ at X direction
D_Y	The translation distance of coordinate $O'_2-X'_2Y'_2Z'_2$ at Y direction
D'_h	Added step displacement of equivalent external gear hob at cutting point h
$D'_h _Y$	Added step displacement of D'_h at Y direction
$\Delta D_{h X}$	Displacement of D'_h at X direction
$D'_h _X$	Added step displacement of D'_h at X direction
θ_m	Rotating angle of equivalent external gear hob at cutting point m
$r_f^{(1)}(\theta_m)$	Radius of gear hob at point m in coordinate $O'_1-X'_1Y'_1Z'_1$
a, b, c, d, m	Points on micro tooth surface of non-circular gear
a', b', c', d'	

1. Introduction

As a gear drive with variable transmission characteristics, non-circular gear is different from conventional ones in tooth profiles and pitch curves, so the geometric, transmission and load characteristics of unconventional gear forms are variable with different transmission functions [1].

Based on the meshing theory of conjugate surface, many scholars did the analysis and optimization for the characteristics of different gear drives. Tang focused on the tooth contact analysis of bevel gear with SGM method revealed the influence properties of different errors (misalignment, fabrication offsets) on the contact results of gear pair [2, 3]. Wang and Sun focused on the computerized research and simulation of epicycloids hypoid gear, proposing the characteristics of contact area and transmission errors, found the epicycloid tooth profile can improve the sensitivity of errors [4, 5]. Taken the relative sliding friction of meshed tooth surface into consideration, the improved contact analysis of spiral bevel gears was made by Tian [6]. F. L. Litvin and Fan presented the shaving computation methods for both spur and helical gears, revealed the trend of contact ellipse for different gear types [7]. The common manufacturing methods for conventional gear types are based on the generating motion of conjugate surface with constant hobbing parameters, the discrete processing traces on target tooth surfaces are even and the roughness is uniform. However, non-circular gear usually rotates with variable radius, causing irregular cutting steps, processes traces and mutative roughness, the conventional machining methods with constant cutting parameters cannot be directly applied on non-circular gears for uniform micro surface.

In order to reduce roughness, improve cutting force and surface precision, a compound generating method with ultrasonic-assisted motion was presented. Yin and Zhao discussed the process of surface grinding with ultrasonic-assisted motion or not, and established a mathematical model for the prediction of grinding force and surface quality [8-10]. Venkatesh considered the surface finishing of bevel gear, presented a finite element simulation for bevel gear with different input parameters [11]. Harpreet proved that the average and maximum surface roughness of bevel gear could be improved to 91.04 % and 71.98 % in an experiment on bevel gear with AISI 1040 carbon steel [12]. Wei and Yang focused on the surface lapping with ultrasonic-assisted motion, found that the material removal rate of ultrasonic lapping is much higher and the surface quality is much better than conventional lapping method [13, 14]. Su investigated the SEM topography of two different Ti6Al4V with the method of conventional milling and ultrasonic-assisted milling, shows the SEM surface roughness can be reduced up to 23.3 % and 19.1 % with UAM method than CM method, and indicates the positive influence of UAM method on surface roughness [15]. An focused on the material removal mechanism of FRCMCs-SiC in machining processes, discussed the influence of process parameters on the machined surface quality, proved that ultrasonic-assisted machining method can reduce cutting force and tool wear, improve machining quality and efficiency [16]. In addition, the experimental turning performance of ultrasonic-assisted turning with textured cutting insert was carried out by Sofuoglu, revealed the

reason for the 35.89 % improvement during ultrasonic-assisted turning as compared to conventional turning [17]. Liu analyzed the wear state of tool in ultrasonic-assisted milling and conventional milling, found that the burr produced by ultrasonic-assisted milling was not obvious and the curl angle of chip generated from ultrasonic-assisted milling was smaller than that from conventional milling in the same wear time, and better surface roughness with lower cutting force and temperature [18]. Due to the benefits of ultrasonic-assisted machining, Amini designed an elliptical ultrasonic-assisted turning model, the better surface finish and lower cutting forces on the turning process of copper with elliptical ultrasonic-assisted motion has been verified by experiment [19].

These results confirmed that the new generating methods with ultrasonic-assisted motion could improve tooth surface roughness obviously. But the basic parameters of non-circular gear are complex and should be derived for surface hobbing with ultrasonic-assisted motion.

Figliolini established the base curve of non-circular gear by the Aronhold theorem, derived the constant pressure angle of this kind of non-circular gear pair [20]. Furthermore, the mathematical model, transmission principle and theoretical simulation model of non-circular gear was presented by F. Y. Zheng et al. [21]. Fuentes proposed two different methods for shaped teeth by face-milling cutters, and analyzed the advantages and disadvantages of the proposed two versions by numerical examples [22].

The above results demonstrate that ultrasonic-assisted processing method is better for surface roughness than normal cutting method, and the specific parameters of non-circular gear can be derived.

This paper compared the two forming methods of non-circular gear with or without ultrasonic-assisted motion, including the mathematical equations of theoretical surface, incremental offset distance and rotating angle of step, micro height and grooves of adjacent cutting points with different parameters. Also, the discussion of the relationship between finished surfaces and cutting methods is covered in this paper. The results provide the theoretical support for further analysis and application of unconventional gear type with complex tooth surface.

2. Surface Hobbing of non-circular gear

2.1. Tooth surface profile of normal gear

With the development and application of gear pair, various processing methods, such as milling, hobbing and so on, have been applied. Based on the simulation processing method proposed by F. L. Litvin [1], the surface hobbing process of normal cylindrical gear can be shown as Fig. 1.

Fig. 1 shows the conjugate generating process of tooth surface. $O_1-X_1Y_1Z_1$, $O_2-X_2Y_2Z_2$ and $O_3-X_3Y_3Z_3$ are fixed coordinates on cylindrical gear, hypothetical generating gear and gear hob respectively. $O'_1-X'_1Y'_1Z'_1$, $O'_2-X'_2Y'_2Z'_2$ and $O'_3-X'_3Y'_3Z'_3$ are movable coordinates on cylindrical gear, hypothetical generating gear and gear hob respectively. β_3 is the rotating angle of movable coordinate $O'_3-X'_3Y'_3Z'_3$ with different meshing point. In Fig. 1(b), $O_3(O'_3)$ keeps a constant distance away from $O_2(O'_2)$ with a distance $O_3O_2 = E$. In the generating process of tooth surface of cylindrical gear, the gear hob is coupled rotating around O_3Z_3 and O_1Z_1 , the tooth flank of gear hob is always the same with tooth flank of hypothetical generating gear (inner gear) and equivalent external gear at point p with coordinate transformation by $O'_3-X'_3Y'_3Z'_3$ to $O'_2-X'_2Y'_2Z'_2$. The mathematical equation $r_p^{(3')}(\theta_p)$ for tooth profile at point p of gear hob can be derived by the tooth profile of hypothetical inner gear or equivalent external gear, shown as:

$$r_p^{(3')}(\theta_p) = r_p^{(2')}(\theta_p) + E, \quad (1)$$

$$\begin{cases} |r_p^{(3')}(\theta_p)||_X = |r_{bp}|[\cos(\theta_{op} + \theta_p) + \theta_p \sin(\theta_{op} + \theta_p)] + |E||_X, \\ |r_p^{(3')}(\theta_p)||_Y = |r_{bp}|[\sin(\theta_{op} + \theta_p) - \theta_p \cos(\theta_{op} + \theta_p)] + |E||_Y, \\ |r_p^{(3')}(\theta_p)||_Z = 0, \end{cases} \quad (2)$$

where p is the common contact point on gear hob, equivalent external gear and hypothetical generating gear, θ_{op} is the starting angle of tooth profile $\theta_{op} = \pi/2z - inv\alpha_o$, θ_p is the range of tooth profile angle, r_{bp} is the basic radius.

According to the pure rolling engagement of those three tooth profiles and conversion matrix $M_{1,2'}$, of the coordinate $O_2'-X_2'Y_2'Z_2'$ to the coordinate $O_1'-X_1'Y_1'Z_1'$, the tooth profile of target gear can be proposed as:

$$\begin{cases} |r_p^{(1')}(\theta_p, \theta_1)||_X = |r_{bp}|[\sin(\theta_{op} + \theta_p + \theta_2 - \theta_1) - \theta_p \cos(\theta_{op} + \theta_p + \theta_2 - \theta_1)] - D_X, \\ |r_p^{(1')}(\theta_p, \theta_1)||_Y = |r_{bp}|[\cos(\theta_{op} + \theta_p + \theta_2 - \theta_1) + \theta_p \sin(\theta_{op} + \theta_p + \theta_2 - \theta_1)] - D_Y, \\ |r_p^{(1')}(\theta_p, \theta_1)||_Z = 0. \end{cases} \quad (3)$$

Eq. (3) illustrates the mathematical equation for target gear, D_Y and D_X are the translation distance of movable coordinate $O_2'-X_2'Y_2'Z_2'$ with meshing from p (rotating angle of cylindrical gear is θ_1) to p' (rotating angle of cylindrical gear is $\theta_1 + \Delta\theta_1$). As described in Fig. 2(b), gear hob always keeps the distance E away from $O_2(O_2')$, so D_Y and D_X can be expressed by the component of arc length $E\beta_3$ in the X or Y directions. Compared with Eq. (2), Eq. (3) has the same form for tooth profile, the target gear is cylindrical gear with the constant radius r_2 .

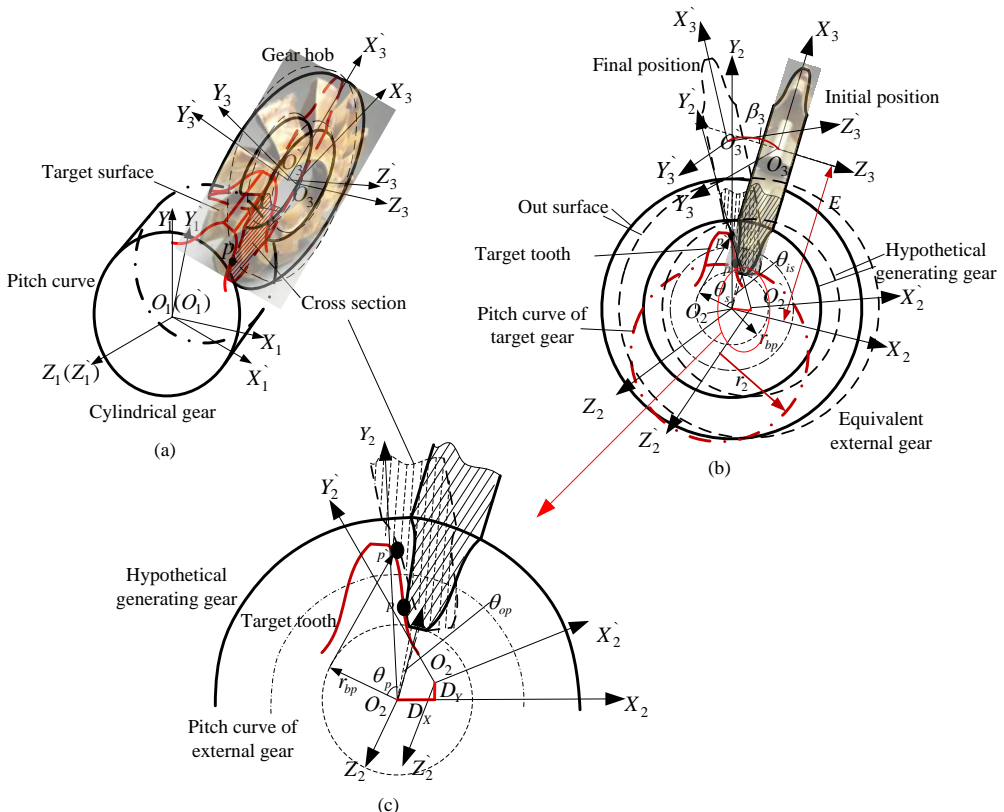


Fig. 1. Theoretical presentation of normal cylindrical gear

2.2. Surface equation of non-circular gear

Based on the conventional Hobbing method of normal cylindrical gear with constant cutting steps, the simulation manufacturing process for non-circular gear tooth profile has been arranged as shown in Fig. 2.

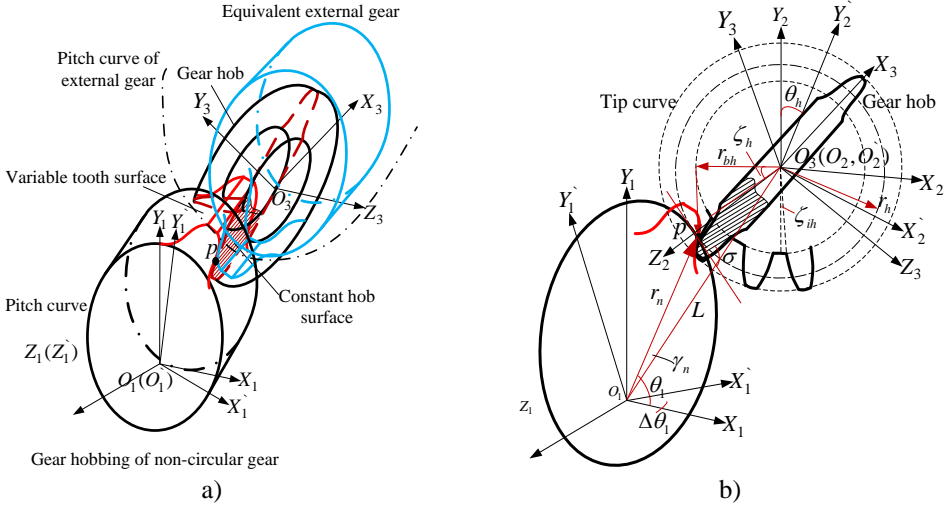


Fig. 2. Simulated hobbing of non-circular gear with conventional method

As shown in Fig. 2(b), the generating profile of gear hob is overlapped with the tooth profile of hypothetical external gear at point p . During the generating process of non-circular gear, the radius $r_n^{(1')}(\theta_n)$ of non-circular gear is angle-varying, related parameters L , γ_n , σ can be derived by external gear rolling on the pitch curve of non-circular gear as:

$$\begin{cases} r_n^{(1')}(\theta_n) = \frac{a(1-e^2)}{(1-ecos\theta_n)}, \\ r_n^{(1)'}(\theta_n) = \frac{d(r_n^{(1')}(\theta_n))}{d(\theta_n)}, \\ \sigma = \arctan\left(\frac{|r_n^{(1')}(\theta_n)|}{|r_n^{(1)'}(\theta_n)|}\right), \\ \gamma_n = \arccos\left(\frac{L^2 + |r_n(\theta_n)|^2 - r_h^2}{(2L|r_n(\theta_n)|)}\right), \\ L = \sqrt{|r_n(\theta_n)|^2 + r_h^2 + 2|r_n(\theta_n)|r_h\sin\sigma}. \end{cases} \quad (4)$$

The coordinate transformation matrix $M_{12'}$, from $O_2'-X_2'Y_2'Z_2'$ to $O_1-X_1Y_1Z_1$ can be established as:

$$M_{12'} = \begin{bmatrix} \cos\theta_h & \sin\theta_h & 0 & L_h\cos(\theta_1 - \gamma_h) \\ -\sin\theta_h & \cos\theta_h & 0 & L_h\sin(\theta_1 - \gamma_h) \\ 0 & 0 & 1 & 0 \\ 0 & 0 & 0 & 1 \end{bmatrix}. \quad (5)$$

Matrix $M_{11'}$, is the coordinate transformation from $O_1-X_1Y_1Z_1$ to $O_1'-X_1'Y_1'Z_1'$ and can be established as:

$$M_{11'} = \begin{bmatrix} \cos(\theta_1) & \sin(\theta_1) & 0 & 0 \\ -\sin(\theta_1) & \cos(\theta_1) & 0 & 0 \\ 0 & 0 & 1 & 0 \\ 0 & 0 & 0 & 1 \end{bmatrix}. \quad (6)$$

In Fig. 2(b), non-circular gear is rotating clockwise while the gear hob is rotating counter-clockwise so the tooth surface of non-circular gear can be proposed as $r_p^{(1')}(\theta_{op}, \theta_p, \theta_1) = M_{12'} \cdot r_p^{(2')}(\theta_{op}, \theta_p)$, and the responded rotating angle θ_h and translation displacements D_h of gear hob can be established as:

$$\begin{cases} |r_h^{(3')} \Delta\theta_h| = \int_{\theta_n}^{\theta_n + \Delta\theta_n} \left(|r_n^{(1')}(\theta_n)|^2 + |r_n^{(1')}(\theta_n)|^2 \right)^{\frac{1}{2}} d\theta_n, \\ \Delta D_h|_x = |r_n^{(1')}(\theta_n + \Delta\theta_n)| \cos(\theta_n + \Delta\theta_n) - |r_n^{(1')}(\theta_n)| \cos(\theta_n), \\ \Delta D_h|_y = |r_n^{(1')}(\theta_n + \Delta\theta_n)| \sin(\theta_n + \Delta\theta_n) - |r_n^{(1')}(\theta_n)| \sin(\theta_n). \end{cases} \quad (7)$$

Taken the parameters of gear hob in Table 1 into Eq. (7), the responded displacement D_h and rotating angle θ_h of equivalent external gear with rotating angle θ_n or $\Delta\theta_n$ of non-circular gear are calculated by MATLAB, illustrated as Fig. 3.

Table 1. Some parameters of gear hob

Parameter	Value
Equivalent modulus m_f (mm)	2
Number of tooth of equivalent external gear z	12
Order of non-circular gear n	1
Distance E (mm)	34
Pressure angle of gear hob α (°)	20

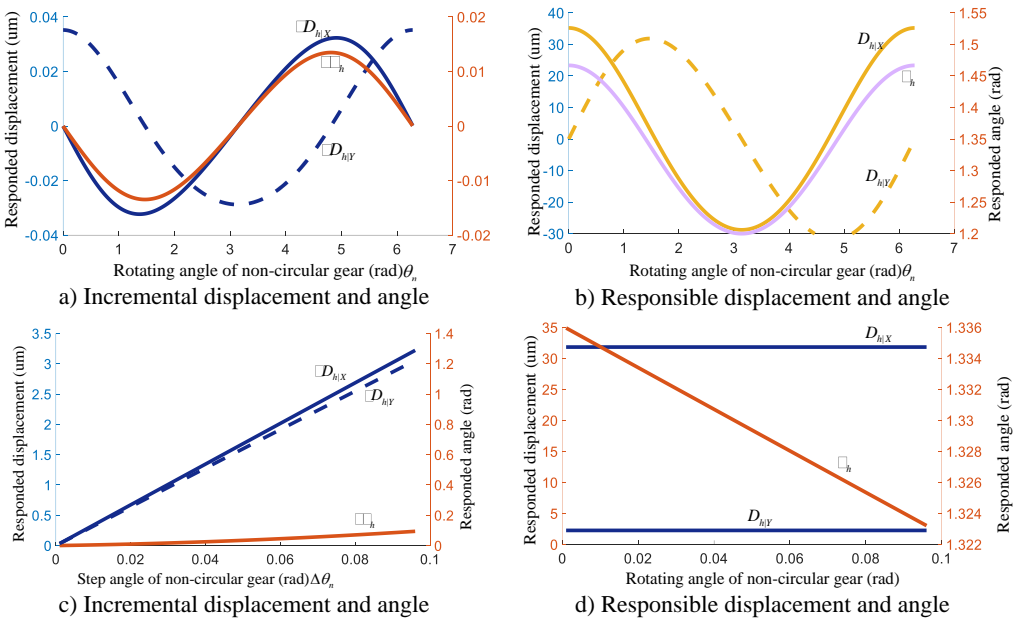


Fig. 3. Displacement D_h and rotating angle θ_h of equivalent external gear

In Fig. 3(a) and (b), the parameters of gear hob and step value are constant, while the value of translation parameters $D_{h|X}$, $D_{h|Y}$, θ_h and step increment $\Delta\theta_h$, $\Delta D_{h|Y}$, $\Delta D_{h|X}$ are variable. In addition, with hobbing goes from short axis to long axis of non-circular gear, the change trend of $D_{h|X}$, $D_{h|Y}$, θ_h and $\Delta\theta_h$, $\Delta D_{h|Y}$, $\Delta D_{h|X}$ are the same with radius of non-circular gear, as Eq. (3). The radius increases from short axis to long axis, the step increment of gear hob will increase with difference growth. Also, the change of translation parameters $D_{h|X}$, $D_{h|Y}$, θ_h will follow the regular pattern of axis. Additionally, $\Delta D_{h|Y}$, $\Delta D_{h|X}$ are range from -0.03 to 0.03 mm and the value of $\Delta\theta_h$ is about 0.018 rad with $\Delta\theta_n = 0.001$ rad. Fig. 3(c) and (d) are values of step parameters with $\Delta\theta_n = 0.01$ rad, demonstrate $D_{h|X}$, $D_{h|Y}$, θ_h and $\Delta\theta_h$, $\Delta D_{h|Y}$, $\Delta D_{h|X}$ are also varying periodically, the lager step value $\Delta\theta_n$, the lager step parameters $D_{h|X}$, $D_{h|Y}$, θ_h and $\Delta D_{h|Y}$, $\Delta D_{h|X}$, $\Delta\theta_h$.

2.3. Surface Hobbing ultrasonic -assisted motion

As shown in Eq. (6) and Fig. 3, the surface roughness and accuracy of non-circular gear are different with different angle θ_n , even the step angle $\Delta\theta_n$ is controlled constant or step increment $\Delta\theta_h$, $\Delta D_{h|Y}$ and $\Delta D_{h|X}$ are obtained accurately. The transmission performance (transmission error, noise, vibration and so on) is limited by surface roughness and accuracy. So the processing method should be improved, taken the range of step increment $\Delta D_{h|Y}$, $\Delta D_{h|X}$ and amplitude of ultrasonic-assisted processing method into consideration, ultrasonic-assisted processing will improve the step increment $\Delta D_{h|Y}$, $\Delta D_{h|X}$ to a certain degree. The manufacturing model with elliptical ultrasonic-assisted method is set up, shown as Fig. 4.

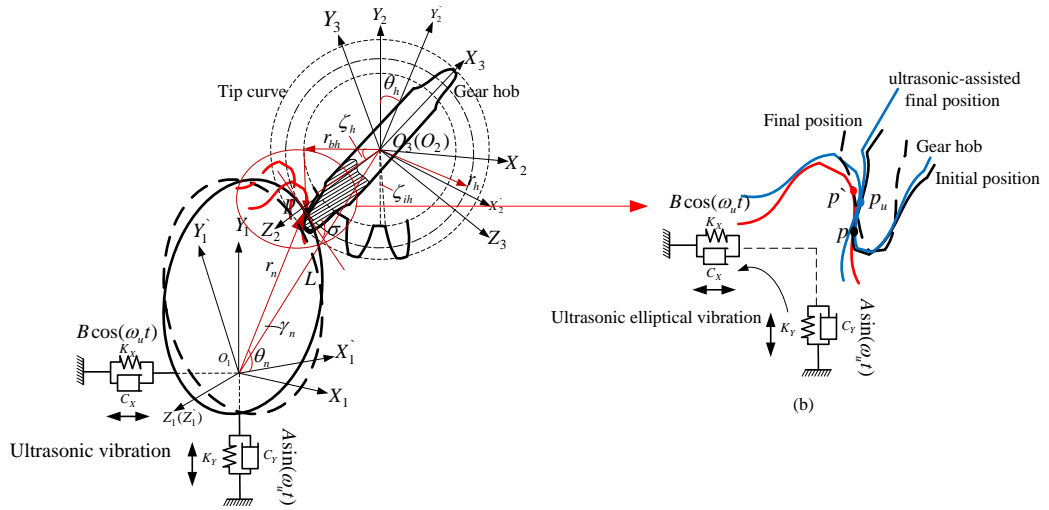


Fig. 4. Ultrasonic-assisted hobbing of non-circular gear

Fig. 3 shows the step distance $\sqrt{(\Delta D_{h|X})^2 + (\Delta D_{h|Y})^2}$ of any adjacent two hobbing points on tooth surface ranges from 0.0315 mm to 0.0355 mm with different θ_n , which will cause machining accuracy unstable by influencing the feed of gear cutter. In order to ensure surface accuracy constant as much as possible, a compound cutting method with ultrasonic-assisted movement are presented. The ultrasonic motion of non-circular gear is established as an elliptical motion with $S_Y = A \sin(\omega_u t)$ at the Y direction and $S_X = B \cos(\omega_u t)$ at the X direction, shown as Fig. 4.

Ultrasonic-assisted motion of gear hob is an elliptical-like ultrasonic vibration with ultra-high frequency. Coupled with the relative rotation and movement between hob and non-circular gear,

the trajectory of cutting point p on tooth surface is actually compound motion. Compared with the rotation and movement of gear hob, the period of elliptical ultrasonic motion is extremely short, and the amplitude is small. It will not change the contact relationship between gear hob and target non-circular gear within a large range, but will improve the step distance as Fig. 4(b). While the high-frequency separation between hob and non-circular gear be ignored, the ultrasonic-assisted responded rotating angle θ'_h and translation displacements D'_h are obtained as:

$$\begin{cases} |r_n^{(1')}(\theta'_n)| = \int_{\theta'_n}^{\theta'_n + \Delta\theta'_n} \left[(|r_n^{(1')}(\theta'_n)| \cos(\theta'_n) + A \sin(\omega_u t))^2 + (|r_n^{(1')}(\theta'_n)| \sin(\theta'_n) + B \cos(\omega_u t))^2 \right]^{1/2} d\theta'_n, \\ |r_n^{(3')}(\theta'_n)| = \int_{\theta'_n}^{\theta'_n + \Delta\theta'_n} (|r_n^{(1')}(\theta'_n)|^2 + |r_n^{(1')'}(\theta'_n)|^2)^{1/2} d\theta'_n, \\ D'_h|_x = |r_n^{(1')}(\theta'_n + \Delta\theta'_n)| \cos(\theta'_n + \Delta\theta'_n) - |r_n^{(1')}(\theta'_n)| \cos(\theta'_n) + B \cos(\omega_u t), \\ D'_h|_y = |r_n^{(1')}(\theta'_n + \Delta\theta'_n)| \sin(\theta'_n + \Delta\theta'_n) - |r_n^{(1')}(\theta'_n)| \sin(\theta'_n) + A \sin(\omega_u t), \end{cases} \quad (8)$$

where $A = 0.005$ mm, $B = 0.004$ mm, θ'_n is the rotating angle of non-circular gear with ultrasonic-assisted method, $\Delta\theta'_n$ is the step angle of non-circular gear and $t = \theta'_n/\omega'_n$, ω'_n is the angular velocity of non-circular gear.

3. Micro tooth surface analysis of non-circular gear

3.1. Micro peak and groove on shaped surface

Compared Eq. (7) and Eq. (8), the responded rotating angle θ'_h , translation displacements $D'_h|_x$ and $D'_h|_y$ are affected by added ultrasonic motion. With the expansion and simplification of Eq. (7), the ultrasonic-assisted values θ'_n and D'_h can be considered as Eq. (7) attached with some extra high frequency and small amplitude expressions.

In the normal forming process, the tooth profile of non-circular gear is created by material removal. Different amount and spacing of removed material make different surface quality as shown in Fig. 5.

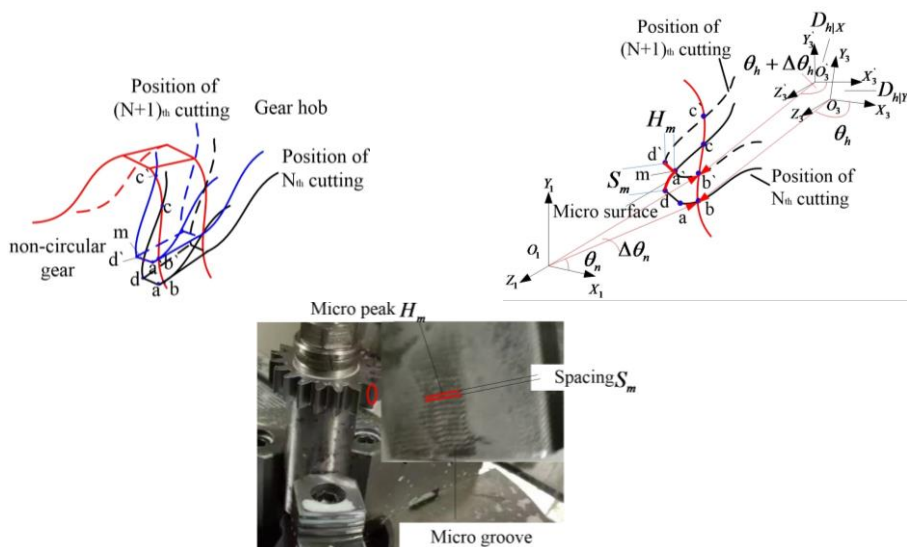


Fig. 5. Micro surface of shaped tooth profile

As shown in Fig. 5, the unsmooth surface is caused by the retained material between two adjacent cutting steps N th and $(N + 1)$ th on non-circular gear blank, making undulating continuous tooth surface as \widehat{abcd} or $a'b'c'd'$ in Fig. 5(b) and (c). Based on the translation displacements Eq. (8), the upper cutting point a , which is shown as micro peak in Fig. 5(c), at N th cutting position can be derived as:

$$\begin{cases} |r_a^{(1')}(\theta_h, \theta_1)|_X = |r_a^{(2')}(\theta_h, \theta_2)|_X \cos(\theta_1 - \theta_2) \\ \quad + |r_a^{(2')}(\theta_h, \theta_1)|_Y \sin(\theta_1 - \theta_2) - D'_h|_X, \\ |r_a^{(1')}(\theta_h, \theta_1)|_Y = -|r_a^{(2')}(\theta_h, \theta_2)|_Y \sin(\theta_1 - \theta_2) \\ \quad + |r_a^{(2')}(\theta_h, \theta_1)|_X \cos(\theta_1 - \theta_2) - D'_h|_Y, \\ |r_a^{(1')}(\theta_h, \theta_1)|_Z = 0. \end{cases} \quad (9)$$

The mathematical expression for the other three points (b, c, d) can be derived by $r_a^{(2')}(\theta_h, \theta_2)$, and the area \widehat{abcd} depicts the material removed at the initial position with angle θ_n . With the same method, the cutting area $a'b'c'd'$ with rotating angle $\theta_n + \Delta\theta_n$ at $(N + 1)$ th cutting point can be built, so the remained material $\widehat{dm'd'}$ between \widehat{abcd} and $a'b'c'd'$ is the unsmooth tooth surface for hobbing step increases from N th to $(N + 1)$ th. The value of micro peak H_m and spacing S_m of micro remained material can be derived as follows:

$$\begin{cases} |r_f^{(1')}(\theta_m)|_X = |r_f| \cos(\theta_m + \zeta_{oh}), \\ |r_f^{(1')}(\theta_m)|_Y = |r_f| \sin(\theta_m + \zeta_{oh}), \\ |r_f^{(1')}(\theta_m)|_Z = 0, \end{cases} \quad (10)$$

$$\begin{cases} |r_m^{(1')}(\theta_m)|_X = |r_{bn}| [\cos(\theta_{on} + \theta_m + \Delta\theta_n) + (\theta_m + \Delta\theta_n) \sin(\theta_{on} + \theta_m + \Delta\theta_n)], \\ |r_m^{(1')}(\theta_m)|_Y = |r_{bn}| [\sin(\theta_{on} + \theta_m + \Delta\theta_n) - (\theta_m + \Delta\theta_n) \cos(\theta_{on} + \theta_m + \Delta\theta_n)], \\ |r_m^{(1')}(\theta_m)|_Z = 0. \end{cases} \quad (11)$$

$r_f^{(1')}(\theta_m)$ is equation for the tip radius of gear hob and $r_f = r_{bp} + (2h_a^* + C^*)m_f$, m_f is equivalent modulus of non-circular gear, $r_m^{(1')}(\theta_m)$ is obtained as an equation for a tooth profile \widehat{cd} at point m on non-circular gear. As a common point between arcs $a'd'$ and \widehat{cd} , the two mathematical expressions for cutting point m should be consistent with each other:

$$\begin{cases} |r_f| \cos(\theta_m + \zeta_{oh}) = |r_{bh}| [\cos(\theta_{on} + \theta_m + \Delta\theta_n) + (\theta_m + \Delta\theta_n) \sin(\theta_{on} + \theta_m + \Delta\theta_n)], \\ |r_f| \sin(\theta_m + \zeta_{oh}) = |r_{bh}| [\sin(\theta_{on} + \theta_m + \Delta\theta_n) - (\theta_m + \Delta\theta_n) \cos(\theta_{on} + \theta_m + \Delta\theta_n)]. \end{cases} \quad (12)$$

With the solution of Eq. (11), the phase angle θ_m of m on hypothetical equivalent external gear can be established by r_{bh} , r_f , ζ_{oh} and $\Delta\theta_n$. Similarly, the micro groove $d(d')$ can be built by the tooth tip point $d(d')$ of gear hob.

3.2. Micro tooth surface with different parameters

As shown in Fig. 5 and Eq. (12), the height of micro peaks, spacing between micro grooves are related to some primary parameters, such as radius r_{bh} , r_f of gear hob, starting angle ζ_{oh} of tooth profile, step length $\Delta\theta_n$, radius $r_n^{(1')}(\theta_n)$ and so on. Taken the processing parameters of gear hob and non-circular gear into Eq. (12), the microscopic micro tooth surface is shown in Fig. 6.

Fig. 6 contains the comparison of micro tooth surface with different methods. Compared Fig. 6(a) and (b), it can be seen that the tooth surface with ultrasonic-assisted vibration is more

regular, the height H_m of micro peak also decreases from 6.5 μm to 2.7 μm with much smaller spacing, making surface roughness much lower. The further variation of micro peak H_m and spacing S_m with different parameters are shown in Fig. 7.

As indicated in Fig. 6, the microfeatures of generated tooth surface can be reflected by the height and width of machining tracks, named as micro peak H_m and spacing S_m in this paper. Fig. 7(a)-(d) illustrate the trend of micro peak H_m and spacing S_m with different parameters.

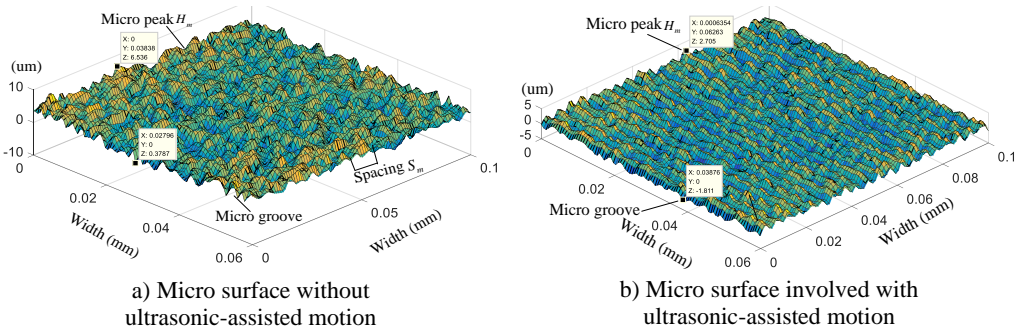


Fig. 6. Micro tooth surface with different methods

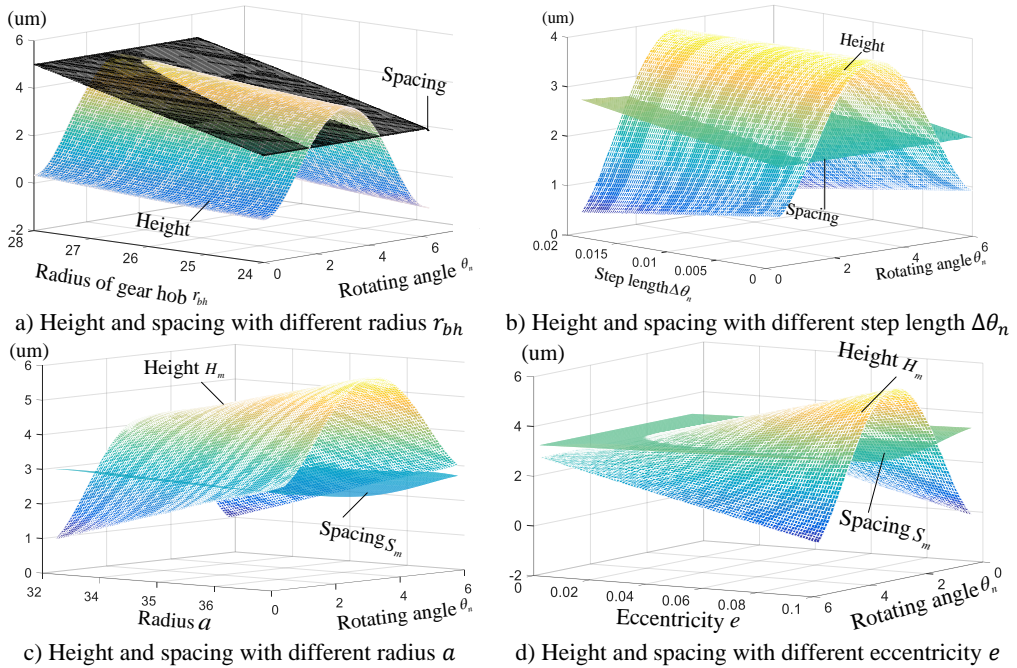


Fig. 7. Micro surface with different control parameters

According to the conjugate generating process in Eq. (11) and Fig. 5, spacing S_m and height H_m are primarily determined by the distance and depth of two adjacent cutting positions. Because of the variable transmission ratio between non-circular gear and equivalent generating gear with variable radius, the constant step angle $\Delta\theta_h$ and depth $|r_{bh}|$ of equivalent generating gear will engender variable $\Delta D_{h|y}$ and $\Delta D_{h|x}$, causing changeable spacing S_m and micro peak H_m .

As shown in Eq. (2), the step distance Δd of two adjacent cutting positions on gear hob can be established as $\Delta d = r_{bh} \cdot \Delta\theta_h$, showing the same trend with radius r_{bh} , while the modulus m_f and tooth number of gear is series values not arbitrary, so the height and thickness of tooth will change with different r_{bh} . Taken these decrease parameters into Eq. (12), the height H_m and spacing S_m

decrease, too. In addition, H_m is not only influenced by the step distance Δd , but also the cutting depth of gear hob and non-circular gear, the thickness of tooth profile, the spacing S_m is merely affected by the step distance, so the change of S_m is more pronounced than it of height H_m with different radius r_{bh} . Based on Eq. (4), with angle θ_n ranges from 0 to 2π , radius increases first and then decreases, so the height H_m on the tooth surface of non-circular gear should be added by the additional values of variable radius $\Delta H_m = \left| |r_n^{(1')}(\theta_n)| - |r_n^{(1')}(\theta_n + \Delta\theta_n)| \right|$ with much obvious range than spacing S_m at the direction of rotating angle θ_n in Fig. 7(a).

The changeable height H_m and spacing S_m create different micro topography on generated tooth surface. H_m mainly influence the height of peaks and spacing S_m influence both the spacing and smoothness of peaks, with radius r_{bh} decrease from 28 mm to 24 mm, the range of H_m changes from $-3.04 \mu\text{m}$ - $4.96 \mu\text{m}$ to $-1.81 \mu\text{m}$ - $2.71 \mu\text{m}$ and the spacing of peaks decrease from 5 μm to 3 μm , causing more regular, compact and obvious peaks. Also, the average error of peaks is improved from 0.96 μm to 0.45 μm , which shows much better regularity and accuracy to the theoretical tooth surface.

Fig. 7(c)-(d) illustrate the further properties of height H_m and width S_m with different parameters: step length $\Delta\theta_n$, radius parameter a and eccentricity e of non-circular gear, getting the similar trend as Fig. 7(a). With the decrease of step length $\Delta\theta_n$, eccentricity e and parameter a , the range of height H_m and spacing S_m decrease with positive correlation. Combined Eq. (12) and Fig. 6-7, it can be seen that the micro topography of tooth surface is mainly affected by the spacing S_m of adjacent cutting tracks and height H_m of cutting peaks, these tracks and peaks are determined by the conjugate relationship between gear hob and non-circular gear, the tooth profile of gear hob, step angle and so on. With the decrease of radius $|r_{bh}|$, step angle $\Delta\theta_n$, eccentricity e and parameter a , the height H_m and spacing S_m decrease, also the average generating error decrease with more regular, compact and clear surface. So the micro topography of non-circular gear is variable and determined by any change of these parameters, showing the relationship between the trend of parameters and micro topography in appendix Table A1.

4. Experiment

For a better understanding and verification of theoretical micro tooth surface of non-circular gear, the experimental hobbing of non-circular gear is operated with cutting parameters in Table 2 and control parameters of non-circular gear in Table 3 with 17Cr2Ni2Mo.

Table 2. Ultrasonic vibration parameters of gear cutter

Parameter	Value
Amplitude A (μm)	5
Amplitude B (μm)	4
Frequency (KHz)	20
spindle speed (r/min)	110
Axial feed speed (mm/r)	0.16
cutting depth (mm/r)	0.05

Table 3. Parameters of non-circular gear

Parameter	Value
Radius factor a (mm)	16
Eccentricity e	0.1
Orders n	1
Rotating speed (r/min)	0.2
Modules (mm)	2

Table 4. Property parameters of 17Cr2Ni2Mo

Parameter	Value
Density (kg/m^3)	8000
Tensile strength (MPa)	≥ 1200
Hardness (HB)	≤ 269
Poisson's ratio	0.30
Yield strength (MPa)	≥ 1080
Thermal conductivity (W m/K)	16.3

As alloy steel with high property parameters, 17Cr2Ni2Mo is often used on gear transmission parts. So this paper focused on the micro surface topography of non-circular gear with two

different cutting methods when machining 17Cr2Ni2Mo under these parameters in Tables 2 to 4.

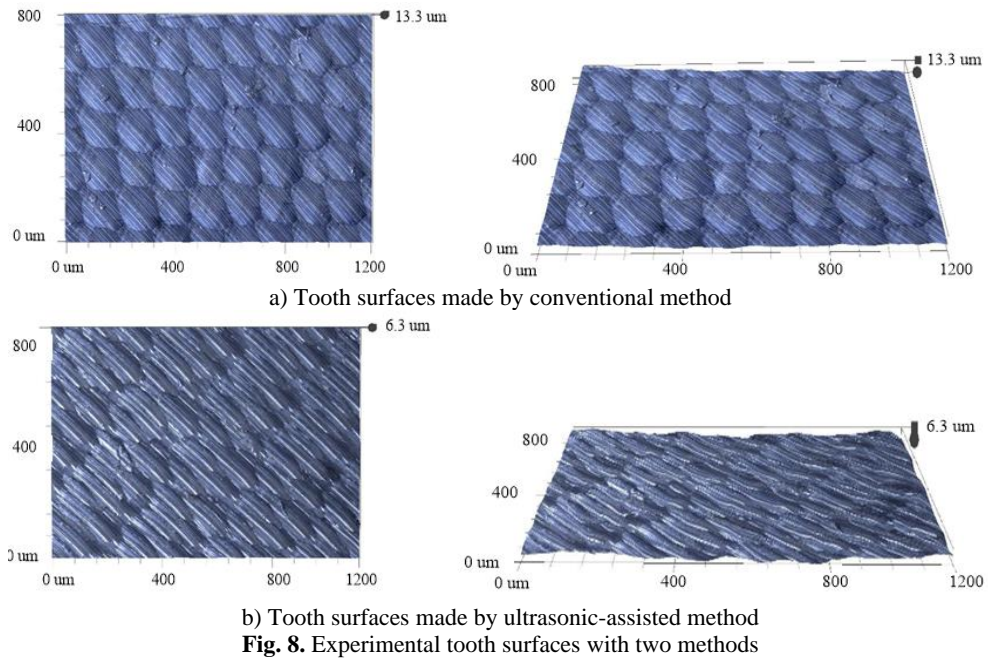


Fig. 8 shows the micro surface of non-circular gear, which were photographed by the Super depth of field 3D microscopy system (VHX-1000C/VW-6000). Comparing the two figures, it can be seen that the machining traces and boundaries of every step during ultrasonic-assisted hobbing are much less than that of conventional fabricating, resulting in lower height H_m and width S_m .

Specifically, the width S_m of adjacent cutting steps with conventional method is obvious, getting a value about 14 μm , which can be considered as the same with theoretical step distance as the parameters in tables. 1 to 3. In addition, the axial feed rate will affect the formed surface periodically, so the micro surface is affected by both cutting steps of gear hob and feed speed of conjugate surfaces, dividing the tooth surface into series of independent areas, and the spacing of every area is about 0.17 mm, which is approximately equal to the feed rate and offset translation distance of gear hob in one rotation. Although the change process among these independent areas is uniform and smooth, the difference of height H_m between micro peak and grooves is large, ranging from 0.3 μm to 6.5 μm , getting the maximum $\Delta H_m = H_m^+ - H_m^- = 6.2 \mu\text{m}$ (H_m^+ is the height of micro peak, and H_m^- is the height of micro groove);

Fig. 8(b) shows the micro surface with ultrasonic vibration, the added motion can perform secondary micro-processing on the boundary surface, cause curling and burrs, make the peaks and boundaries of cutting trajectory be more obvious. But it will break the peaks with large micro cutting, reducing the height of peak to $-0.3\text{-}2.7 \mu\text{m}$.

Although the peaks and grooves on micro surface are more compact with more burrs in ultrasonic-assisted hobbing process than that in normal hobbing methods, the roughness and topographic error is smaller with the same after cutting condition and stabilization, which can be consistent as the same with the conclusions in REFs. [18] and [19].

5. Conclusions

According to the friction theory of conjugate surfaces, the transmission stability, lubrication, vibration will be affected by the micro topography of tooth surface. Based on the variable radius $r_n^{(1)}(\theta_n)$ of non-circular gear, the step translation $D'_h|_x$, $D'_h|_y$ and rotating angle $\Delta\theta_h$ of gear hob

are variable in the hobbing process, causing variable surface roughness. So the improved manufacturing method with ultrasonic-assisted motion was presented for surface hobbing of non-circular gear. The further conclusions are shown as follows:

In the generating process, all the parameters will affect the micro tooth surface of non-circular gear (r_{bh} , ζ_{oh} , r_f , m_f , z of gear hob and a , e , n , θ_n of non-circular gear). Although the parameters of gear hob and step value are constant, the value of translation parameters $D_{h|X}$, $D_{h|Y}$, θ_h and step increment $\Delta\theta_h$, $\Delta D_{h|Y}$, $\Delta D_{h|X}$ are variable with the same trend as the radius of non-circular gear, shown as Fig. 3 and Eq. (3). Concretely, the radius increase from short axis to long axis, the translation parameters, θ_h and step increment $\Delta D_{h|Y}$, $\Delta D_{h|X}$, $\Delta\theta_h$ of gear hob will increase with difference growth, getting $D_{h|X}$ and $D_{h|Y}$ range from -0.03 to 0.03 mm and maximum $\Delta\theta_h$ about 0.018 rad with $\Delta\theta_n = 0.001$ rad.

Taken the formed tooth surface with conventional method in Fig. 8(a) into Eq. (6) and Fig. 6, the boundaries of every cutting step is obvious with a value about 14 μm , shows the same width with theoretical step distance. Moreover, the axial feed rate will affect the formed surface periodically, divide the micro tooth surface into series of independent areas, and the spacing of every area is about 0.17 mm, which is approximately equal to the feed rate and offset translation distance of gear hob. The change process among these independent areas is uniform and smooth, but the difference of height H_m between micro peak and grooves is large, ranging from 0.3 μm to 6.5 μm , getting the maximum $\Delta H_m = H_m^+ - H_m^- = 6.2$ μm .

While the surface with ultrasonic vibration method in Fig. 8(b) shows much small independent areas, means the boundaries of cutting trajectory are more obvious, and the change ratio of height H_m is more drastic. But the added vibration motion will do a secondary micro-processing on the manufactured surface, breaking the peaks with large micro cutting, the super depth photo result indicates the secondary micro-processing will added on the peak topography and reduce the height H_m from 0.3 - 6.5 μm to -0.3 - 2.7 μm .

Although the ultrasonic micro-processing will generate additional machining tracks, cause more curling and burrs, the roughness and topographic error is smaller than those in conventional method during the same cutting condition and stabilization. So the compound hobbing method with ultrasonic-assisted motion will improve the micro tooth surface of non-circular gear obviously.

Acknowledgements

The authors gratefully acknowledge the support by the Science and Research Program of Chongqing Municipal Education Commission (No. KJQN202101514) and the Science Fund Project of Chongqing University of Science and Technology (No. ckrc2021006) for our investigations.

Data availability

The datasets generated during and/or analyzed during the current study are available from the corresponding author on reasonable request.

Conflict of interest

The authors declare that they have no conflict of interest.

References

- [1] C. J. He and C. Lin, "Analysis of loaded characteristics of helical curve face gear," (in Chinese), *Mechanism and Machine Theory*, Vol. 115, pp. 267–282, 2017, <https://doi.org/10.1016/j.mechmachtheory.2017.05.014>

- [2] J. Y. Tang, Y. F. Lu, and C. Zhou, "Error tooth contact analysis of spiral bevel gears transmission," (in Chinese), *Chinese Journal of Mechanical Engineering*, Vol. 44, No. 7, pp. 18–23, 2008, <https://doi.org/10.3321/j.issn:0577-6686.2008.07.003>
- [3] J. Y. Tang, Y. F. Lu, and C. Zhou, "Research on improved tooth contact analysis algorithm of spiral bevel gears," (in Chinese), *Journal of Aerospace Power*, Vol. 24, No. 1, pp. 189–195, 2009.
- [4] F. Wang et al., "Tooth contact analysis of epicycloid hypoid gear considering assembly misalignment," (in Chinese), *Transactions of the Chinese Society for Agricultural Machinery*, Vol. 43, No. 9, pp. 213–218, 2012, <https://doi.org/10.6041/j.issn.1000-1298.2012.09.039>
- [5] Y. H. Sun and X. H. Li, "Spread-out helix modified roll of spiral bevel gears and tooth contact analysis," (in Chinese), *Journal of Tianjin University (Science and Technology)*, Vol. 50, No. 4, pp. 421–428, 2017, <https://doi.org/10.11784/tdxbz201605042>
- [6] X. B. Tian and Z. D. Fang, "A new method for loaded tooth contact analysis (LTCA) of spiral bevel gears with friction," (in Chinese), *Journal of Northwestern Polytechnical University*, Vol. 18, pp. 19–22, 2000, <https://doi.org/10.3969/j.issn.1000-2758.2000.01.005>
- [7] F. L. Litvin, Q. Fan, D. Vecchiato, A. Demenego, R. F. Handschuh, and T. M. Sep, "Computerized generation and simulation of meshing of modified spur and helical gears manufactured by shaving," *Computer Methods in Applied Mechanics and Engineering*, Vol. 190, No. 39, pp. 5037–5055, Jul. 2001, [https://doi.org/10.1016/s0045-7825\(00\)00362-5](https://doi.org/10.1016/s0045-7825(00)00362-5)
- [8] L. Yin, B. Zhao, B. Huo, W. Bie, and C. Zhao, "Analytical modeling of grinding force and experimental study on ultrasonic-assisted forming grinding gear," *The International Journal of Advanced Manufacturing Technology*, Vol. 114, No. 11-12, pp. 3657–3673, Jun. 2021, <https://doi.org/10.1007/s00170-021-07086-3>
- [9] W. B. Bie et al., "Overview and expectation on gear anti – fatigue manufacture by ultrasonic-assisted machining," (in Chinese), *Surface Technology*, Vol. 47, No. 7, pp. 35–51, 2018, <https://doi.org/10.16490/j.cnki.issn.1001-3660.2018.07.006>
- [10] W. Bie, B. Zhao, C. Zhao, L. Yin, and X. Guo, "System design and experimental research on the tangential ultrasonic vibration-assisted grinding gear," *The International Journal of Advanced Manufacturing Technology*, Vol. 116, No. 1-2, pp. 597–610, Sep. 2021, <https://doi.org/10.1007/s00170-021-07459-8>
- [11] G. Venkatesh, A. K. Sharma, and P. Kumar, "On ultrasonic assisted abrasive flow finishing of bevel gears," *International Journal of Machine Tools and Manufacture*, Vol. 89, pp. 29–38, Feb. 2015, <https://doi.org/10.1016/j.ijmactools.2014.10.014>
- [12] H. Singh and P. K. Jain, "Study on ultrasonic-assisted electrochemical honing of bevel gears," *Proceedings of the Institution of Mechanical Engineers, Part B: Journal of Engineering Manufacture*, Vol. 232, No. 4, pp. 705–712, Mar. 2018, <https://doi.org/10.1177/0954405416654086>
- [13] B. Y. Wei, X. Z. Deng, and Z. D. Fang, "Study on ultrasonic-assisted lapping of gears," *International Journal of Machine Tools and Manufacture*, Vol. 47, No. 12-13, pp. 2051–2056, Oct. 2007, <https://doi.org/10.1016/j.ijmactools.2005.11.003>
- [14] J. J. Yang, H. Zhang, X. Z. Deng, and B. Y. Wei, "Ultrasonic lapping of hypoid gear: System design and experiments," *Mechanism and Machine Theory*, Vol. 65, pp. 71–78, Jul. 2013, <https://doi.org/10.1016/j.mechmachtheory.2013.03.002>
- [15] Y. Su and L. Li, "Surface integrity of ultrasonic-assisted dry milling of SLM Ti6Al4V using polycrystalline diamond tool," *The International Journal of Advanced Manufacturing Technology*, Vol. 119, No. 9-10, pp. 5947–5956, Apr. 2022, <https://doi.org/10.1007/s00170-022-08669-4>
- [16] Q. An, J. Chen, W. Ming, and M. Chen, "Machining of SiC ceramic matrix composites: A review," *Chinese Journal of Aeronautics*, Vol. 34, No. 4, pp. 540–567, Apr. 2021, <https://doi.org/10.1016/j.cja.2020.08.001>
- [17] M. A. Sofuoğlu et al., "Numerical investigation of hot ultrasonic assisted turning of aviation alloys," *Journal of the Brazilian Society of Mechanical Sciences and Engineering*, Vol. 40, No. 3, pp. 1–12, Mar. 2018, <https://doi.org/10.1007/s40430-018-1037-4>
- [18] Q. Liu, J. Xu, and H. Yu, "Experimental study of tool wear and its effects on cutting process of ultrasonic-assisted milling of Ti6Al4V," *The International Journal of Advanced Manufacturing Technology*, Vol. 108, No. 9-10, pp. 2917–2928, Jun. 2020, <https://doi.org/10.1007/s00170-020-05593-3>
- [19] S. Amini, M. Khosrojerdi, and R. Nosouhi, "Elliptical ultrasonic-assisted turning tool with longitudinal and bending vibration modes," *Proceedings of the Institution of Mechanical Engineers, Part B:*

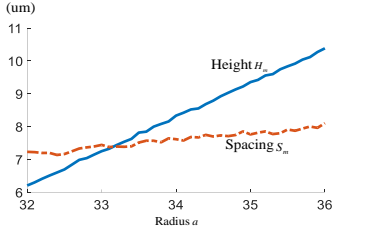
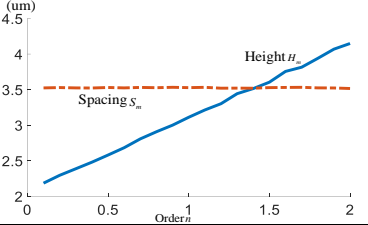
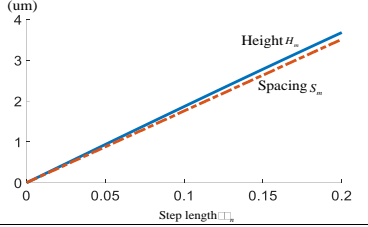
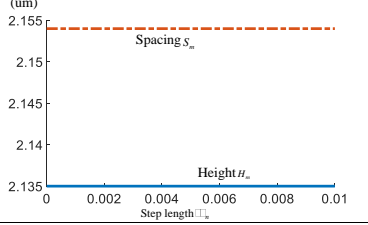
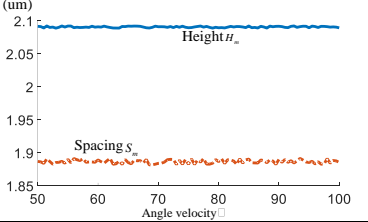
Journal of Engineering Manufacture, Vol. 231, No. 8, pp. 1389–1395, Jun. 2017, <https://doi.org/10.1177/0954405415592196>

- [20] G. Figliolini, H. Stachel, and J. Angeles, “Base curves of involute cylindrical gears via Aronhold’s first theorem,” *Proceedings of the Institution of Mechanical Engineers, Part C: Journal of Mechanical Engineering Science*, Vol. 230, No. 7-8, pp. 1233–1242, Apr. 2016, <https://doi.org/10.1177/0954406215612814>
- [21] A. Fuentes, R. Ruiz-Orzaez, and I. Gonzalez-Perez, “Computerized design, simulation of meshing, and finite element analysis of two types of geometry of curvilinear cylindrical gears,” *Computer Methods in Applied Mechanics and Engineering*, Vol. 272, pp. 321–339, Apr. 2014, <https://doi.org/10.1016/j.cma.2013.12.017>
- [22] F. Zheng, L. Hua, and X. Han, “The mathematical model and mechanical properties of variable center distance gears based on screw theory,” *Mechanism and Machine Theory*, Vol. 101, pp. 116–139, Jul. 2016, <https://doi.org/10.1016/j.mechmachtheory.2016.03.005>

Appendix

Table A1. Micro surface with different single parameter

Sorts	Parameter	Height H_m and spacing S_m	Trend and range
Gear hob	Radius r_{bh}		H_m increased obviously S_m constant slightly
	Module m_f		H_m increased obviously S_m constant slightly
	Tooth number Z		H_m decreased obviously S_m decreased slightly
Non-circular gear	Eccentricity e		H_m increased obviously S_m increased slightly

	Radius a		H_m increased obviously S_m increased obviously
	Order n		H_m increased obviously S_m increased slightly
Step length $\Delta\theta_n$	$\Delta\theta_n = k\theta + C$ and $\Delta\theta_n = C$		H_m increased obviously S_m increased obviously
	$\Delta\theta_n = \sum_{i=0}^k b_i \theta_n^i$		H_m constant S_m constant
Angle velocity ω	$\omega = C$ $\omega = k\theta + C$ and $\omega = \sum_{i=0}^k d_i \theta_n^i$		H_m constant S_m constant



Chunjiang He received his Ph.D. degree in School of Mechanical Engineering, Chongqing University, Chongqing, China, in 2020. Now he works at School of Mechanical and Power Engineering, Chongqing University of science and technology. His current research interests include Mechanical Design Computer Aided Engineering, Design and Precision manufacturing of new gear transmission and micro-nano transmission, et al.



Chao Lin received his Ph.D. degree in School of Mechanical Engineering, Chongqing University, Chongqing, China, in 2002. Now he works at School of Mechanical Engineering, Chongqing University. His current research interests include Mechanical Design Computer Aided Engineering, Design and manufacture of new gear transmission and micro-nano transmission, Product digital design and manufacturing, et al.